Chemical Engineering Journal 155 (2009) 175–183

Contents lists available at ScienceDirect

Chemical Engineering Journal

journal homepage: www.elsevier.com/locate/cej

Theoretical and experimental SO_2 adsorption onto pistachio-nut-shell activated carbon for a fixed-bed column

Aik Chong Lua*, Ting Yang

School of Mechanical and Aerospace Engineering, Nanyang Technological University, 50 Nanyang Avenue, Singapore 639798, Republic of Singapore

ARTICLE INFO

Article history:
Received 22 January 2009
Received in revised form 10 July 2009
Accepted 14 July 2009

Keywords:
Activated carbon
Adsorption model
Fixed-bed column
Sulphur dioxide
Breakthrough curve
Finite-difference method

ABSTRACT

The adsorption and desorption behaviours of SO_2 onto activated carbons, which were prepared from pistachio-nut shells, were studied theoretically and experimentally in a fixed-bed column. A mathematical model considering non-equilibrium, non-isothermal and non-adiabatic effects for a single gas adsorbate on a fixed-bed system was derived and the model was solved by a finite-difference method. A linear driving force (LDF) approximation is used for heat and mass transfer rates. The temperature-dependent Langmuir equilibrium isotherm is used to represent gas–solid equilibrium isotherm. The theoretical study was conducted to compare the present model with the isothermal and adiabatic model. The effects of inlet concentration, flow rate and temperature were studied experimentally. These experimental data showed that the breakthrough time decreased with increasing feed concentration, increasing flow rate and increasing temperature and the trends were correctly predicted by the model calculations.

1. Introduction

Adsorption of gases and liquids onto solid adsorbents has great environmental significance since it can effectively remove pollutants from both aqueous and gaseous streams. In recent years, the fixed-bed or column adsorption has been applied increasingly to solvent recovery or air purification and large-scale separations, like pressure swing adsorption and temperature swing adsorption. To design an appropriate adsorption process, detailed information of the column dynamics are required. The dynamics behaviour of an adsorption column system may be classified according to the nature of the mass front and the complexity of the mathematical model required to describe the system. The nature of the mass transfer front is determined solely by the form of the equilibrium relationship while the complexity of the mathematical model depends on the concentration level, the choice of rate equation and the choice of flow model. Ruthven [1] provided a detailed classification scheme.

There are a number of column models developed over the years under various simplified assumptions. Most of them deal with a single adsorbate for both isothermal [2–4] and non-isothermal systems [5–8]. There were also studies for multi-component adsorption [9–11]. The fixed-bed adsorption for bulk component system was also investigated by Hwang et al. [12].

However, most of experimental data in the afore-mentioned studies were investigated for systems consisting of adsorbate of hydrocarbon or carbon dioxide/carbon monoxide and adsorbent of commercial activated carbon or zeolite. Few studies have been reported on SO_2 adsorption onto a column packed with activated carbons. This paper presents a general model (non-equilibrium, non-isothermal and non-adiabatic conditions) for gaseous adsorption in a column bed of adsorbents and the solutions to the model using a finite-difference method. The numerical solutions were then verified with experimental results for SO_2 adsorption onto activated carbons prepared from pistachio-nut shells in a fixed column bed configuration.

2. Model outline

The model is based on an adsorption column packed with porous spherical adsorbent particles through which an inert carrier gas flows at a steady rate. At time zero, a steady concentration of an adsorbable gas is introduced at the column inlet. After the breakthrough is complete, the adsorbable gas is withdrawn from the feed and the equilibrated bed is regenerated by desorption. The following assumptions are made.

i) The concentration of the adsorbable gas component is small.
ii) The frictional pressure drop through the bed is negligible.
iii) The adsorption equilibrium isotherm is represented by a temperature-dependent Langmuir isotherm.
iv) The mass transfer rate is represented by a linear driving force expression.
v) The flow pattern is described by the axial dispersive flow model.

* Corresponding author. Tel.: +65 6790 5535; fax: +65 6792 4062.
E-mail address: maclua@ntu.edu.sg (A.C. Lua).

1385-8947/$ – see front matter © 2009 Elsevier B.V. All rights reserved.
doi:10.1016/j.cej.2009.07.031

Nomenclature

a_a	ratio of the external surface area to the volume of column wall ($a_a = 2R_{w2}/(R_{w2}^2 - R_{w1}^2)$)
a_s	ratio of particle external surface area to volume ($a_s = 3/R_p$)
a_{w1}	ratio of the internal surface area to the volume of column ($a_{w1} = 2/R_{w1}$)
a_{w2}	ratio of the internal surface area to the volume of column wall ($a_{w2} = 2R_{w1}/(R_{w2}^2 - R_{w1}^2)$)
b	Langmuir constant at temperature T
b_0	Langmuir constant at temperature T_0
c	adsorbate concentration in the gas phase
c_0	adsorbate concentration in the feed
c_{in}	adsorbate concentration at the inlet of column
C_g	heat capacity of the gas
C_s	heat capacity of the adsorbent
C_w	heat capacity of the wall
D_m	molecular diffusivity
D_L	axial mass dispersion coefficient
d_p	particle diameter
h_a	heat transfer coefficient from wall to ambient
h_s	film heat transfer coefficient
h_w	overall effective coefficient of the wall heat transfer
k	effective mass transfer coefficient
K_g	gas thermal conductivity
K_{e0}	effective thermal conductivity of a quiescent bed
K_L	effective axial bed thermal conductivity
K_s	solid thermal conductivity (adsorbent)
L	length of column
Nu	Nusselt number ($Nu = (h_s d_p)/K_g$)
Pe	particle Peclet number ($Pe = Vd_p/D_L$)
Pe_h	heat transfer column Peclet number ($Pe_h = (VL\rho_g C_g)/K_L$)
Pe_m	mass transfer column Peclet number ($Pe_m = VL/D_L$)
Pr	Prandtl number ($Pr = C_g\mu/K_g$)
Q	dimensionless adsorbate concentration in the solid phase ($Q = q/q_0$)
Q^*	dimensionless equilibrium adsorbate concentration in the solid phase ($Q^* = q^*/q_0$)
q	adsorbate concentration in the solid phase
q_0	value of q at equilibrium with c_0 at T_0
q_m	saturation constant at Langmuir isotherm
q^*	value of q at equilibrium with c at T
R_g	gas constant
R_p	radius of particle
R_{w1}	internal column radius
R_{w2}	external column radius
Re	Reynolds number ($Re = (\rho_g \varepsilon_b V d_p)/\mu$)
Sc	Schmidt number ($Sc = \mu/(\rho_g D_m)$)
t	time
T	temperature of adsorption
T_a	ambient temperature
$\bar{T}_a$	dimensionless ambient temperature ($\bar{T}_a = T_a/T_0$)
T_g	temperature in the gas phase
$\bar{T}_g$	dimensionless temperature in the gas phase ($\bar{T}_g = T_g/T_0$)
T_s	temperature in the solid phase
$\bar{T}_s$	dimensionless temperature in the solid phase ($\bar{T}_s = T_s/T_0$)
T_w	temperature at the column wall
$\bar{T}_w$	dimensionless temperature at the column wall ($\bar{T}_w = T_w/T_0$)
T_0	feed temperature
V	interstitial velocity
x	dimensionless axial column coordinate ($x = z/L$)
Y	dimensionless adsorbate concentration in the gas phase ($Y = c/c_0$)
z	axial coordinate in the bed
$(-\Delta H)$	heat of adsorption
ε_b	bed porosity
μ	dynamic viscosity of gas
ρ_g	bulk density of the gas
ρ_p	apparent density of the adsorbent
ρ_w	density of the column wall
τ	dimensionless time ($\tau = Vt/L$)

vi) The amount of carrier gas adsorbed is negligible.
vii) The radial velocity, temperature and concentration gradients across the bed cross-section are negligible.
viii) The temperature within a particle is uniform.
ix) The adsorbent particles are spherical in shape.
x) The physical properties of the gas throughout the column are based on those of the feed gas and the physical properties of the adsorbent and the column wall remain unchanged.

The governing equations for the adsorption system are given below. The symbols are defined in the nomenclature.

Mass balance for the gas phase is:

$$-D_L\frac{\partial^2 c}{\partial z^2} + V\frac{\partial c}{\partial z} + \frac{\partial c}{\partial t} + \frac{1-\varepsilon_b}{\varepsilon_b}\rho_p\frac{\partial q}{\partial t} = 0 \quad (1)$$

The energy balance for the gas phase includes the heat transfer to the solid phase and to the column wall.

$$-\varepsilon_b K_L\frac{\partial^2 T_g}{\partial z^2} + V\varepsilon_b\rho_g C_g\frac{\partial T_g}{\partial z} + \varepsilon_b\rho_g C_g\frac{\partial T_g}{\partial t} + (1-\varepsilon_b)a_s h_s(T_g - T_s) + a_{w1}h_w(T_g - T_w) = 0 \quad (2)$$

The energy balance for the solid phase includes the heat generated by the adsorption of the adsorbate.

$$\rho_p C_s\frac{\partial T_s}{\partial t} = a_s h_s(T_g - T_s) + \rho_p(-\Delta H)\frac{\partial q}{\partial t} \quad (3)$$

The energy balance for the column wall includes the heat transfer from the gas phase and to the atmosphere.

$$\rho_w C_w\frac{\partial T_w}{\partial t} = h_w a_{w2}(T_g - T_w) + h_a a_a(T_a - T_w) \quad (4)$$

In the above equations, the heat transfer rates are expressed as linear function of overall driving forces. Similarly, the mass transfer rate of gas and solid phase can be represented by the linear driving force (LDF) model:

$$\frac{\partial q}{\partial t} = k(q^* - q) \quad (5)$$

The LDF model is a lumped-parameter model for particle adsorption. Hwang and Lee [2] had used the LDF model to determine the adsorption and desorption breakthrough behaviours of carbon monoxide and carbon dioxide on activated carbon. They concluded that the experimental adsorption and desorption curves could be predicted fairly well by the LDF model. Hence, the LDF model is used for the SO_2 adsorption and desorption tests in this study and its suitability will be verified by the comparison between model predictions and experimental results later on. In this study, a constant LDF mass transfer coefficient is used and such an assumption is generally accepted as fairly accurate.

The equilibrium adsorption capacity q^*, in turn, is given by the equilibrium adsorption isotherm. In this study, the temperature-dependent Langmuir isotherm was used to represent the gas–solid equilibrium isotherm.

$$q^* = q_m \frac{b(T_g)c}{1 + b(T_g)c} \tag{6}$$

$$b = b_0 \exp\left(\frac{-\Delta H}{R_g T}\right) \tag{7}$$

The associated initial conditions are as follows. For $0 < z < L$:

$$c(0,z) = 0,\ c_{in} = c_0,\ q(0,z) = 0,\ T_g(0,z) = T_s(0,z) = T_w(0,z) = T_0\ (\text{adsorption}) \tag{8}$$

$$c(0,z) = c_0,\ c_{in} = 0,\ q(0,z) = q_0,\ T_g(0,z) = T_s(0,z) = T_w(0,z) = T_0\ (\text{desorption}) \tag{9}$$

and the boundary conditions at $z = 0$ and $z = L$ for $t > 0$ are:

$$D_L \left.\frac{\partial c}{\partial z}\right|_{z=0} = V(c - c_{in}) \tag{10}$$

$$\left.\frac{\partial c}{\partial z}\right|_{z=L} = 0 \tag{11}$$

$$K_L \left.\frac{\partial T_g}{\partial z}\right|_{z=0} = V\rho_g C_g (T_g - T_0) \tag{12}$$

$$\left.\frac{\partial T_g}{\partial z}\right|_{z=L} = 0 \tag{13}$$

The following non-dimensional variables and parameters [7,8,12] are defined below.

$$Y = \frac{c}{c_0};\ Q = \frac{q}{q_0};\ Q^* = \frac{q^*}{q_0} \tag{14}$$

$$\overline{T_g} = \frac{T_g}{T_0};\quad \overline{T_s} = \frac{T_s}{T_0};\quad \overline{T_w} = \frac{T_w}{T_0};\quad \overline{T_a} = \frac{T_a}{T_0} \tag{15}$$

$$x = \frac{z}{L};\quad \tau = \frac{Vt}{L} \tag{16}$$

$$Pe_m = \frac{VL}{D_L} \tag{17}$$

$$Pe_h = \frac{VL\rho_g C_g}{K_L} \tag{18}$$

$$\Phi = \frac{1 - \varepsilon_b}{\varepsilon_b}\rho_p \frac{q_0}{c_0} \tag{19}$$

$$\alpha = \frac{kL}{V} \tag{20}$$

$$\delta = \frac{-\Delta H}{R_g T_0} \tag{21}$$

$$\lambda = \frac{q_0}{q_m} \tag{22}$$

$$\gamma_1 = \frac{L(1 - \varepsilon_b)a_s h_s}{\varepsilon_b V \rho_g C_g} \tag{23}$$

$$\gamma_2 = \frac{a_{w1} h_w L}{\varepsilon_b V \rho_g C_g} \tag{24}$$

$$\gamma_3 = \frac{a_s h_s L}{V \rho_p C_s} \tag{25}$$

$$\gamma_4 = \frac{(-\Delta H) q_0}{C_s T_0} \tag{26}$$

$$\gamma_5 = \frac{a_{w2} h_w L}{V \rho_w C_w} \tag{27}$$

$$\gamma_6 = \frac{a_a h_a L}{V \rho_w C_w} \tag{28}$$

In non-dimensional form, the mass balance equation Eq. (1) becomes:

$$\frac{\partial^2 Y}{\partial x^2}\frac{1}{Pe_m} = \frac{\partial Y}{\partial x} + \frac{\partial Y}{\partial \tau} + \Phi \frac{\partial Q}{\partial \tau} \tag{29}$$

The energy balance equations (2), (3) and (4) for gas phase, solid phase and column wall will transform into dimensionless forms as given in Eqs. (30), (31) and (32), respectively.

$$\frac{\partial^2 \overline{T_g}}{\partial x^2}\frac{1}{Pe_h} = \frac{\partial \overline{T_g}}{\partial x} + \frac{\partial \overline{T_g}}{\partial \tau} + \gamma_1(\overline{T_g} - \overline{T_s}) + \gamma_2(\overline{T_g} - \overline{T_w}) \tag{30}$$

$$\frac{\partial \overline{T_s}}{\partial \tau} = \gamma_3(\overline{T_g} - \overline{T_s}) + \gamma_4 \frac{\partial Q}{\partial \tau} \tag{31}$$

$$\frac{\partial \overline{T_w}}{\partial \tau} = \gamma_5(\overline{T_g} - \overline{T_w}) + \gamma_6(\overline{T_a} - \overline{T_w}) \tag{32}$$

The mass transfer rate equation Eq. (5) becomes:

$$\frac{\partial Q}{\partial \tau} = \alpha \left\{ \frac{\exp[\delta((1/\overline{T_g}) - 1)]Y}{1 - \lambda\{1 - \exp[\delta((1/\overline{T_g}) - 1)\}Y} - Q \right\} \tag{33}$$

The simultaneous solutions to Eqs. (29)–(33) with initial and boundary conditions will yield the adsorption and desorption breakthrough curves and the temperature profiles.

3. Methods and procedures for numerical solutions

The dynamic equations for the non-equilibrium, non-isothermal and non-adiabatic process with single component adsorbate consist of five partial differential equations (PDEs) for the mass and energy balances within the column. All these equations are non-linear PDEs and coupled with one another. Therefore, numerical methods are required to solve these equations. In this study, a finite-different method was used [13,14]. To carry out the discretization, the implicit backward difference (for convection items, i.e. $\partial Y/\partial x$, $\partial \overline{T_g}/\partial x$, etc.) and the central difference (for dispersion items, i.e. $\partial^2 Y/\partial x^2$, $\partial^2 \overline{T_g}/\partial x^2$) were applied. The discretized equations for mass and energy balances are all tridiagonal systems which can be easily solved by the Gauss elimination method. Assuming that all the variables (namely, Q_i^n, Y_i^n, $\overline{T_{g_i}}^n$, $\overline{T_{s_i}}^n$, $\overline{T_{w_i}}^n$, where the subscripts i and n refer to the spatial and time variables respectively) are known, the values of Q_i^{n+1}, Y_i^{n+1}, $\overline{T_{g_i}}^{n+1}$, $\overline{T_{s_i}}^{n+1}$, $\overline{T_{w_i}}^{n+1}$ can be found iteratively and then the procedure is repeated until the desired degree of convergence is achieved. The finite-different implicit method is given in Appendix A. To solve the above equations, a program written in FORTRAN was developed. The Gaussian elimination scheme based on the main element chosen and a finite-difference implicit method were adopted. The final solution was stable. The numerical computation was performed using the AMD K6-2 400 MHZ computer and the average CPU time was about 60–600 s depending on the particular case.

4. Parameter estimation

In order to simulate the column dynamics and compare the simulations with the experimental response curves, the numerical values for the dimensionless parameters are required. The physical and thermodynamic properties of the gas phase were assumed to be those of the feed gas at the inlet temperature. Therefore, the densities, specific heat capacities and thermal conductivities for the gas, the solid phase and the column wall were obtained from available

Table 1
Parameters used in bed column simulations.

Parameter	Unit	Values
Column length (L)	cm	20
Internal column radius (R_{w1})	mm	5
External column radius (R_{w2})	mm	6
Column porosity		0.62
Density of column wall (ρ_w)	kg/m^3	7800
Heat capacity of column wall (C_w)	J/(kg K)	462
Particle radius (R_p)	mm	0.75
Particle porosity		0.51
Apparent density of particle (ρ_p)	kg/m^3	1.01
Heat capacity of particle (C_s)	J/(kg K)	900
Thermal conductivity of particle (K_s)	W/(m K)	0.58
Heat capacity of gas (C_g)	J/(kg K)	1020
Density of gas (ρ_g)	kg/m^3	1.25
Thermal conductivity of gas (K_g)	W/(m K)	0.026
Viscosity of gas (μ)	kg/(m s)	17.86×10^{-6}
Heat of adsorption ($-\Delta H$)	kJ/mol	15.8
Langmuir isotherm constant (b) at 25 °C	m^3 gas/mol	22.68
Langmuir isotherm saturation constant (q_m)	mol/kg C	1.805

physical properties. Bed porosity, bed length, bed diameter, particle diameter, fluid velocity, feed concentration and temperature were directly measurable operating quantities. Table 1 shows the complete set of physical, thermodynamic and process parameters used for the column study.

The axial mass dispersion coefficient (D_L) was estimated from the correlation of Hsu and Haynes [15].

$$\frac{1}{\mathrm{Pe}} = \frac{0.328}{ReSc} + \frac{3.33}{1 + 0.59(ReSc)^{-1}} \tag{34}$$

The effective axial bed thermal conductivity (K_L) was estimated according to Wakao and Kaguei [16].

$$\frac{K_L}{K_g} = \frac{K_{e0}}{K_g} + 0.5PrRe \tag{35}$$

$$\frac{K_{e0}}{K_g} = \left(\frac{K_s}{K_g}\right)^n \quad \text{with } n = 0.280 - 0.757\log_{10}\varepsilon_b - 0.057\log_{10}\left(\frac{K_s}{K_g}\right) \tag{36}$$

The film heat transfer coefficient h_s was also estimated from Wakao and Kaguei [16].

$$\mathrm{Nu} = 2 + 1.1Pr^{1/3}Re^{0.6} \tag{37}$$

The heat transfer coefficient from wall phase to ambient, h_a, was selected as 2.1 W/(m^2 K) for stainless steel column [12,17]. The mass transfer coefficient (k) and the overall wall heat transfer coefficient (h_w) were the two remaining unknowns which were determined by matching the experimental breakthrough curves for varying concentrations and temperatures with the simulation results.

5. Experimental system

5.1. Fixed-bed experiment

A column for the adsorption of SO_2 onto the activated carbons was used for the experimental studies. Sulphur dioxide with different concentrations was selected as the adsorbate whilst the activated carbon adsorbent was prepared from the pistachio-nut shell. The preparation of the activated carbon from pistachio-nut shell was reported elsewhere by the authors [18]. The physical properties of the activated carbon are shown in Table 2. Nitrogen was used as the carrier gas and helium was used as the purge gas during desorption.

Table 2
Physical properties of activated carbon prepared from pistachio-nut shell.

True density	2.05 g/cm^3
Apparent density	1.01 g/cm^3
Total porosity	0.51
Micropore porosity	0.16
Macropore porosity	0.35
Radius of particle	0.75 mm
Radius of microsphere	1.325×10^{-9} m
Average macropore diameter	3.36×10^{-8} m
BET(N_2) surface area	1064 m^2/g

The schematic diagram of the experimental set-up for the column tests is shown in Fig. 1. It consisted of three parts: gas cylinder and pipe, adsorption column, and data collection and analysis. The 200 mm long and 10 mm internal diameter adsorption column was fabricated from stainless steel material. Heating elements with variable power output were wrapped around the column to vary the temperature during adsorption and desorption. Fine meshes were installed at both ends of the adsorption column to ensure uniform gas distribution and prevent the carry-over of the adsorbent particles.

Three K-type thermocouples installed at the mid-length and the two ends of the packed column were connected to a temperature data acquisition system (34970A, HP) so that continuous monitoring of the column temperature could be achieved. The gas flow rate was controlled by a flow meter which was pre-calibrated using the soap bubble technique. The concentration history at the exit of the column was continuously detected by a SO_2 gas analyser (MLT1, Fisher-Rosemount) equipped with a non-dispersive infrared-photometer and connected to a data recording system (LTVTE008, TrendView). The temperature and concentration data acquisition and recording system were both linked to a personal computer with corresponding software to process the data.

Column test was operated in the up-flow mode. Prior to the experiment, the activated carbon was subjected to or regenerated at 350 °C under vacuum for the whole night. At an adjusted flow rate, helium gas was used to purge the column for a sufficiently long time to allow the gas analyser baseline to stabilize and the column temperature to become uniform. The helium gas was then replaced by the feed gas (SO_2 with nitrogen as a carrier gas) through the three-way valve. This could be considered as a step change. The effluent concentration was continuously monitored by the gas analyser and recorded on the TrendView recorder to obtain the breakthrough curve. The adsorption breakthrough was completed if the bed was thoroughly saturated with the feed. The feed gas was then cut off and the desorption curve was obtained using a helium purge at a higher temperature of 353 K.

5.2. Equilibrium measurement

The equilibrium adsorption capacity of sulphur dioxide by the activated carbon prepared from pistachio-nut shell was determined by a thermo-gravimetric analyzer. Adsorption isotherms at different temperatures are shown in Fig. 2. It can be seen that the Langmuir isotherms match the experimental data well over a range of concentrations and temperatures. The extracted values of b using Eq. (6) with q_m constant, were obtained as shown in Table 3. The

Table 3
Values of Langmuir isotherm constant at various temperatures.

Temp. (°C)	b (m^3 gas/mol)
25	22.68
50	14.72
80	8.068
100	6.52

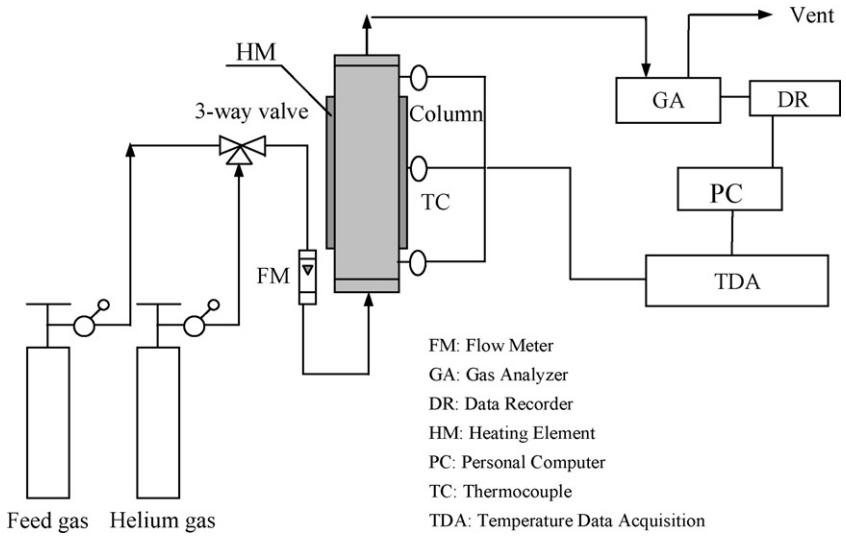

Fig. 1. Schematic diagram of the experimental set-up for column tests.

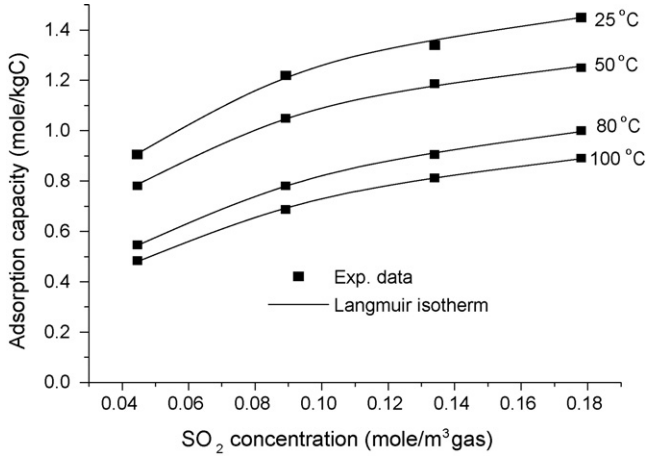

Fig. 2. SO_2 adsorption isotherms for the activated carbons at different temperatures.

heat of adsorption, $-\Delta H$, was determined by fitting the Langmuir isotherm equilibrium constant b to the van't Hoff equation:

$$b = b_0 \exp\left(\frac{-\Delta H}{R_g T}\right) \tag{38}$$

The heat of adsorption of SO_2, $-\Delta H$, was determined to be 15.8 kJ/mol. This value is close to that estimated by Wakao and Kaguei [16], which is 15 kJ/mol. This value is also of the same order of magnitude as the $(-\Delta H)$ value of 22.6 kJ/mol (for Norit RB commercial activated carbon) obtained by Gray and Do [19]. The difference may be due to the different physical and chemical properties of the various adsorbents.

6. Results and discussion

6.1. Theoretical study

In the numerical simulations, a temperature of 25 °C, a concentration of 1000 ppm and a flow rate of 345 cm^3/min were used as the reference conditions to carry out the runs. Using the data from Table 1 and the correlations for the axial mass dispersion coefficient D_L (Eq. (34)), the axial bed thermal conductivity K_L (Eq. (35)) and the film heat transfer coefficient h_s (Eq. (37)), the following reference values were used for the simulation runs:

$D_L = 5.6 \times 10^{-4}\ m^2/s$, $K_L = 0.15\ W/(m\,K)$, $h_s = 92\ W/(m^2\,K)$, $h_a = 2.1\ W/(m^2\,K)$

The mass transfer coefficient k and the overall wall heat transfer coefficient h_w were fitted and selected as $0.08\ s^{-1}$ and $42\ W/(m^2\,K)$ respectively for the purpose of simulations. These values are comparable to those from other studies [10,12,20].

6.1.1. Column concentration and temperature profiles

The numerical simulations can be used to gain some insight into the processes occurring inside the adsorption column by observing the variations in the concentration and temperature profiles within the column. Fig. 3(a) and (b) show the model simulations of concentration and temperature profiles respectively using the reference conditions. The concentration and temperature fronts move progressively towards the outlet of the column with time. For the concentration profiles, Fig. 3(a), a constant pattern quickly forms, which shows that the shape of the mass transfer zone remains the same. Furthermore, all the concentration profiles show steep falls across the mass transfer zones. These two phenomena are due to the favourable nature of the isotherm. As the adsorption progresses up the column, the temperature peak propagates through the column due to the moving of the location where the adsorption takes place. During the initial stage (for example, τ less than 4200), the adsorption has just started. Therefore, both the mass and heat transfers are in the developing stages with a lower temperature peak observed. When the column is nearly depleted (for example, τ more than 25,200), there is almost no further adsorption resulting in a breakthrough of the column and a very low temperature rise.

Another observation is that for the same time interval, the thermal wave travels a longer distance than the concentration wave. For example, when $\tau = 4200$, the concentration front has just reached to $x = 0.3$, but the thermal front has reached to $x = 0.9$. This is because for most gas systems (applicable to the present reference conditions), the ratio of $(q_0/c_0)/(C_s/C_g)$ is more than 1 which results in the thermal wave running ahead of the mass transfer wave. This ratio is a measure of the velocity of the thermal wave to the velocity of the concentration wave. If the adsorption is strong, the concentration wave will travel slower as compared to the thermal wave, making this ratio greater than 1.

Since the ratio of $(q_0/c_0)/(C_s/C_g)$ is very much greater than 1, a pure thermal wave is formed. The natural velocity of the con-

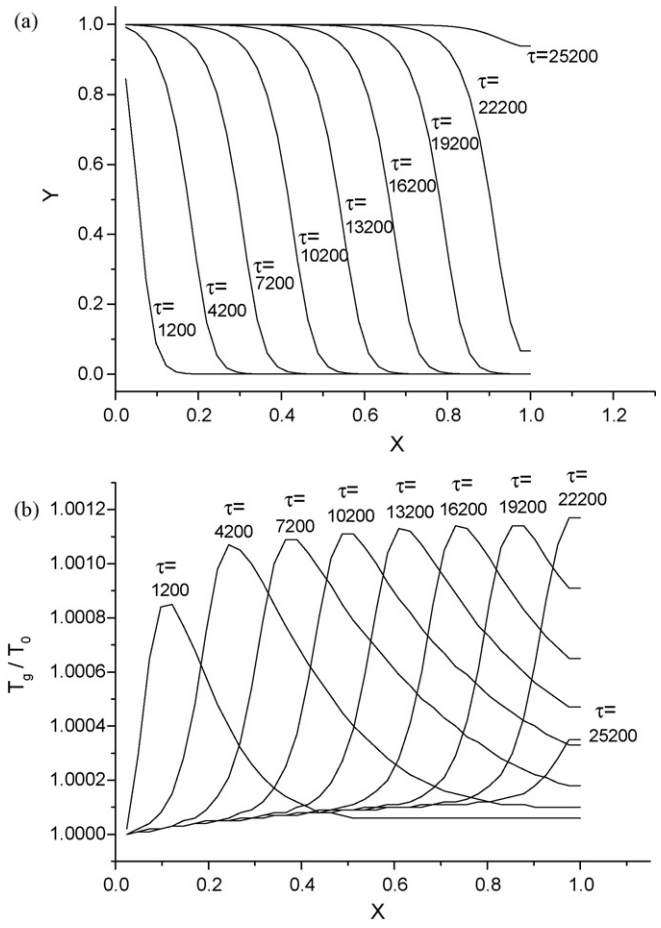

Fig. 3. Simulations of (a) column concentration, and (b) temperature profiles at different times (Φ = 25,000).

centration wave lags behind that of the thermal wave so that the change of temperature has no much effect on the concentration curves. Of course, another reason is that if the temperature change (Fig. 3(b)) were examined, it is too small to have an effect on the concentration profile. In order to show the effect of temperature on the concentration curve, a combined thermal-concentration wave should form instead of a pure thermal wave. For subsequent simulations, $(q_0/c_0)/(C_s/C_g)$ was then drastically decreased (reflected in the simulations where Φ was changed from 25,000 to 50). Simulations were carried out to show the different cases of bed profiles which are presented next.

6.1.2. Comparison of isothermal, non-isothermal–adiabatic and non-isothermal–non-adiabatic column profiles

Fig. 4(a), (b) and (c) show the bed profiles for (i) isothermal, (ii) non-isothermal and non-adiabatic, and (iii) non-isothermal and adiabatic cases, respectively, using the parameters for the reference conditions (i.e. temperature of 25 °C, 1000 ppm concentration and 345 cm^3/min flow rate) except that Φ is reduced from 25,000 to 50 to manifest the effect of temperature on the bed profiles. Fig. 4(b) is simulated from the present model which is based on the non-isothermal and non-adiabatic conditions. In these figures, the dimensionless equilibrium amount of adsorbate, Q^*, is calculated from the isotherm equation for the corresponding concentration and temperature.

The concentration profiles of the present model (non-isothermal and non-adiabatic conditions) in Fig. 4(b) are similar to those of the isothermal case in Fig. 4(a) although the isothermal case produces slightly steeper concentration profiles (notably the Q^* curve)

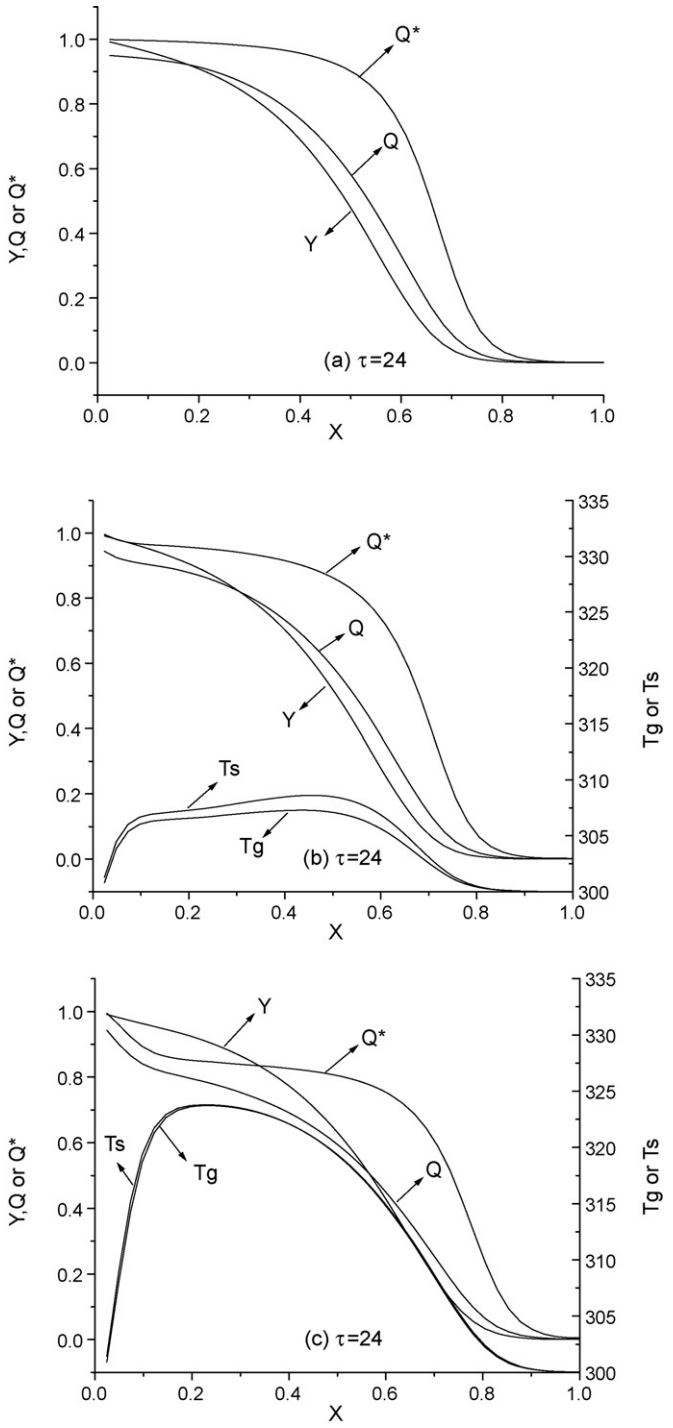

Fig. 4. Bed profiles of various dependent variables at τ = 24 for (a) isothermal case, (b) non-isothermal and non-adiabatic case, and (c) non-isothermal and adiabatic case (Φ = 50).

than the non-isothermal and non-adiabatic case. However, the intense interaction between the temperature and the concentration within the column causes the generation of relatively broader concentration profiles of gas and solid for the non-isothermal and adiabatic case (Fig. 4(c)) and well-defined plateaus in the temperature curves for the non-isothermal cases (Fig. 4(b) and (c)). For the non-isothermal cases, the concentration profiles are broader than those of the isothermal case of Fig. 4(a) due to the heat of adsorption in the former. In addition, the maximum temperature rise in the non-adiabatic model is much lower than in the adiabatic model

Table 4
Adsorption column operating conditions.

Run No.	Type	Y_0 (ppm)	F^* (cm^3/min)	Temperature (K)	Adsorbate	Purge gas	k (s^{-1})
AD1	Adsorption	1000	345	298	SO_2	-	0.08
AD2	Adsorption	3000	345	298	SO_2	-	0.10
AD3	Adsorption	4000	345	298	SO_2	-	0.11
AD4	Adsorption	4000	274	298	SO_2	-	0.11
AD5	Adsorption	4000	410	298	SO_2	-	0.11
AD6**	Adsorption	1000	345	353	SO_2	-	0.15
AD7**	Desorption		345	353	-	He	0.15

* F (flow rate) was measured at 1 atm and 298 K.
** AD6 and AD7 were cyclic and sequential steps of adsorption and desorption runs.

due to the heat transfer effect through the column wall in the former. For the non-isothermal cases, the comparison between the gas and solid phase concentration profiles shows that the solid phase concentration profiles (especially Q^*) have plateau zones, indicating that Q^* and Q are more significantly affected by temperature effects than the gas phase concentration which was also reported by Hwang et al. [12]. The formation of this plateau zone for the solid phase concentration (especially Q^*) is because the equilibrium concentration Q^* is dependent not only on the gas concentration but also on the temperature. Thus, the effect of decreasing temperature will counteract the effect of decreasing gas concentration in the downstream part of the mass transfer zone, giving rise to the plateau zone for solid phase concentration. As a result of the finite mass transfer resistance and the finite film heat transfer resistance (k and h_s reflected in the model), Q^* and T_s are always greater than Q and T_g respectively.

6.2. Comparison of experimental data with simulation results

Measuring the temperatures along the column using thermocouples (Fig. 1), the temperature field was observed to be constant for the different experimental conditions used in this study. Therefore, it suffices to use the isothermal model for comparison with the experimental data instead of the more elaborate non-isothermal and non-adiabatic model. Seven adsorption and desorption runs of SO_2 sorption on the activated carbons prepared from pistachio-nut shells were conducted in order to study the influences of flow rate, adsorbate concentration and adsorption temperature on the performance of the adsorption column. The experimental results were used to compare with the simulation results to test the validation of the model established. Details of the operation conditions for the adsorption column system are given in Table 4.

A typical adsorption–desorption cycle for SO_2 sorption is shown in Fig. 5. The results showed that the isothermal model provided a reasonably good match for both the adsorption and desorption curves especially for adsorption. The calculated mass transfer coefficient (k) which fits the adsorption and desorption curves well for each run is given in Table 4. For the desorption curve, there is a small divergence from the model at the tail-end part. This could be that the same set of parameters used for the adsorption simulations were also used for the desorption case in which some of the experimental conditions were different. Fig. 5 also shows that the breakthrough time (380 min) is longer than the depletion time (about 60 min = 530–470 min). The desorption curve is significantly broader, having a longer tail than the adsorption breakthrough curve. This difference is due to the nature of the equilibrium isotherm. Since the adsorption isotherm is favourable as shown in Fig. 2, then the isotherm is unfavourable for desorption, hence in Fig. 5, the adsorption will result in a steeper breakthrough curve and a broader depletion curve for the desorption process.

The effect of gas flow rate on the breakthrough curve for the same gas temperature and concentration is shown in Fig. 6. The agreement between the model and the three breakthrough curves

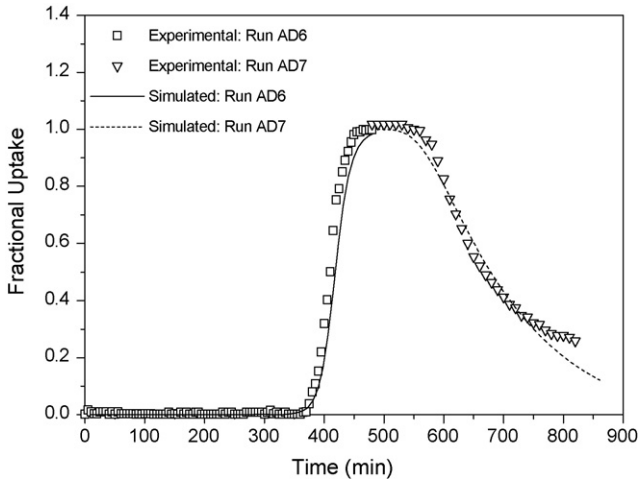

Fig. 5. Experimental curves for column tests for SO_2 adsorption and desorption. Run AD6—adsorption, Run AD7—desorption .

is good. The very small increase of axial mass dispersion coefficient due to increasing flow rate or gas velocity (when the flow rate was increased from 274 to 410 cm^3/min, D_L only increased from 4.39×10^{-4} to 6.7×10^{-4} m^2/s) did not significantly affect the shape of the breakthrough curves for the conditions studied, which was also reported by Silva and Rodrigues [20]. However, the higher flow rate resulted in earlier breakthrough of the adsorbate. It is physically expected as more flow rate will convey more adsorbate into the bed per unit time.

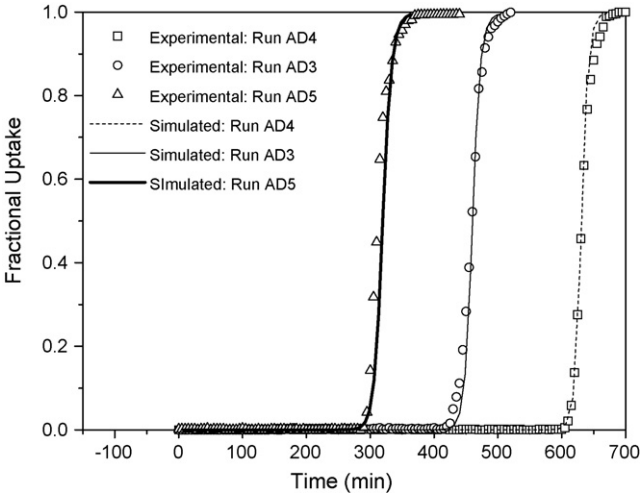

Fig. 6. Effects of flow rate on experimental breakthrough curves and simulation results. Run AD4: flow rate = 274 cm^3/min, Run AD3: flow rate = 345 cm^3/min, Run AD5: flow rate = 410 cm^3/min.

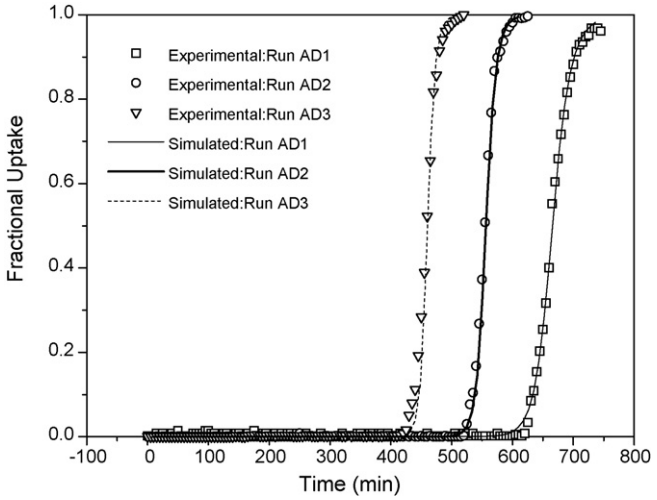

Fig. 7. Effects of feed concentration on experimental breakthrough curves and simulation results. Run AD1: concentration = 1000 ppm, Run AD2: concentration = 3000 ppm, Run AD3: concentration = 4000 ppm.

Fig. 7 shows the effect of feed concentration on the breakthrough curve for the same gas temperature and flow rate. For a favourable isotherm as in this case, the ratio of adsorbed phase to fluid phase concentration decreased with increasing fluid concentration or in other words, the higher feed concentration would result in a relative smaller degree of sorption capacity such that an earlier breakthrough of adsorption and a relatively steeper breakthrough curve would result. On the other hand, increasing feed concentration increased the effective mass transfer coefficient k which could be seen from Table 4. This is expected as the effective mass transfer coefficient is contributed by micropore diffusion, macropore diffusion, surface diffusion as well as the external film diffusion. Increasing feed concentration increases the surface diffusion so that the mass transfer coefficient would increase, giving rise to steeper breakthrough curve. This trend is correctly reflected in the experimental data in Fig. 7 and furthermore, the simulation results agree well with the experimental data.

The effect of temperature on the breakthrough curve for the same gas flow rate and concentration is shown in Fig. 8. Increasing temperature greatly decreases the adsorption capacity due to the nature of the adsorption process (exothermic) so that an earlier breakthrough curve would occur. Although at a higher temperature, the isotherm becomes less favourable which would result in a broader breakthrough curve, the increasing effective mass transfer coefficient k (see Table 4) due to increasing micropore and macropore diffusion with temperature would make the breakthrough curve more abrupt. Thus, the overall effect was that the temperature had little influence on the shape of the breakthrough curve for the conditions studied here. Fig. 8 also shows that the model simulations agree well with the experimental results.

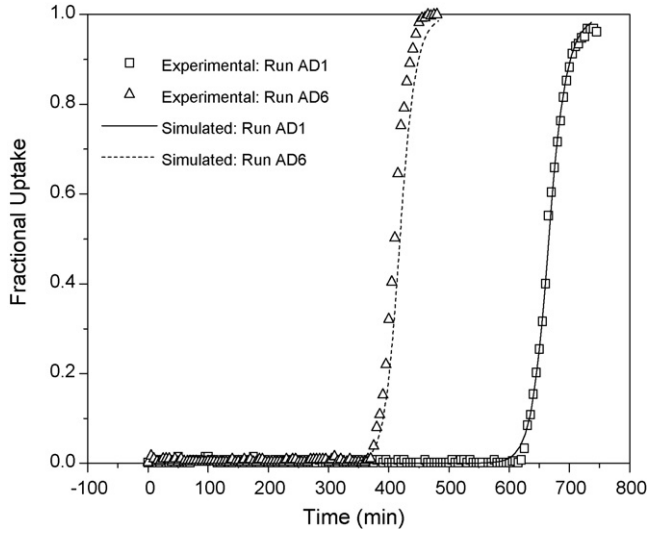

Fig. 8. Effects of temperature on experimental breakthrough curves and simulation results. Run AD1: temperature = 298K, Run AD6: temperature = 353K.

From the simulations and experimental results presented, it can be concluded that the mathematical model proposed in the present study provides a good representation of the experimentally observed behaviour of breakthrough curve for SO_2 adsorption/desorption on activated carbons prepared from pistachio-nut shells. Thus, the model does indeed represent the essential features of the real system.

7. Conclusions

A mathematical model (non-equilibrium, non-isothermal and non-adiabatic) for single component adsorption on a fixed-bed system was developed and solved by a finite-difference method. The concentration and temperature of bed profiles were investigated from the model calculations and compared with isothermal, non-isothermal and non-adiabatic, and non-isothermal and adiabatic model simulations. Concentration profiles for the isothermal and the non-isothermal and non-adiabatic models were similar. The breakthrough curves of SO_2 onto activated carbons prepared from pistachio-nut shells were measured experimentally. The effects of inlet concentration, flow rate and temperature were also studied experimentally. Experimental data clearly show that the shape of the breakthrough and desorption curves are practically influenced by the adsorption equilibrium isotherm. Due to insignificant temperature variations along the small diameter column as experimentally determined, the experimental breakthrough curves were compared with those simulated from the isothermal model. Good agreement was found between the model predictions and the experimental results.

Appendix A.

The dynamic equations for the non-equilibrium, non-isothermal and non-adiabatic model for a single component adsorbate in a column of adsorbents can be solved using the finite-difference implicit method. To carry out the discretisation, the implicit backward difference (for convection items, i.e. $\partial Y/\partial x$, $\partial \overline{T_g}/\partial x$, etc.) and central difference (for dispersion items, i.e. $\partial^2 Y/\partial x^2$, $\partial^2 \overline{T_g}/\partial x^2$) are applied as follows:

$$\left(\frac{\partial Y}{\partial \tau}\right)_{i,n+1} = \frac{Y_{i,n+1} - Y_{i,n}}{\Delta \tau} \tag{A1}$$

$$\left(\frac{\partial Y}{\partial x}\right)_{i,n} = \frac{Y_{i+1,n} - Y_{i-1,n}}{2\,\Delta x} \tag{A2}$$

$$\left(\frac{\partial^2 Y}{\partial x^2}\right)_{i,n} = \frac{Y_{i+1,n} - 2Y_{i,n} + Y_{i-1,n}}{\Delta x^2} \tag{A3}$$

where the subscripts i and n refer to the spatial and time variables, respectively (the derivatives of $\overline{T_g}$, $\overline{T_s}$, $\overline{T_w}$, Q are similar to those of Y).

Assuming the column is divided into N intervals with $N+1$ grid points (with $i = 1$ at $x = 0$ and $i = N+1$ at $x = 1$), substituting Eqs. (A1), (A2) and (A3) into Eqs. (29), (30), (31), (32) and (33), the following

discretised equations for mass and energy balances are obtained:

$$Y_i^{n+1}\left(\frac{2}{\Delta x^2 \mathrm{Pe_m}}+\frac{1}{\Delta x}+\frac{1}{\Delta\tau}\right) = Y_{i+1}^{n+1}\frac{1}{\Delta x^2\mathrm{Pe_m}}+Y_{i-1}^{n+1}\left(\frac{1}{\Delta x}+\frac{1}{\Delta x^2\mathrm{Pe_m}}\right) + \frac{Y_i^n}{\Delta\tau}-\Phi\frac{Q_i^{n+1}-Q_i^n}{\Delta\tau} \quad 2\le i\le N \tag{A4}$$

$$Y_i^{n+1}\left[\frac{2}{\Delta x^2\mathrm{Pe_m}}+\frac{1}{\Delta x}+\frac{1}{\Delta\tau}+(\Delta x\mathrm{Pe_m}-1)\left(\frac{1}{\Delta x}+\frac{1}{\Delta x^2\mathrm{Pe_m}}\right)\right] = Y_{i+1}^{n+1}\frac{1}{\Delta x^2\mathrm{Pe_m}}+\Delta x\mathrm{Pe_m}\left(\frac{1}{\Delta x}+\frac{1}{\Delta x^2\mathrm{Pe_m}}\right) + \frac{Y_i^n}{\Delta\tau}-\Phi\frac{Q_i^{n+1}-Q_i^n}{\Delta\tau} \quad i=1\,(\text{for adsorption}) \tag{A5}$$

$$Y_i^{n+1}\left[\frac{2}{\Delta x^2\mathrm{Pe_m}}+\frac{1}{\Delta x}+\frac{1}{\Delta\tau}+(\Delta x\mathrm{Pe_m}-1)\left(\frac{1}{\Delta x}+\frac{1}{\Delta x^2\mathrm{Pe_m}}\right)\right] = Y_{i+1}^{n+1}\frac{1}{\Delta x^2\mathrm{Pe_m}}+\frac{Y_i^n}{\Delta\tau}-\Phi\frac{Q_i^{n+1}-Q_i^n}{\Delta\tau} \quad i=1\,(\text{for desorption}) \tag{A6}$$

$$Y_i^{n+1}=Y_{i+1}^{n+1} \quad i=N \tag{A7}$$

$$\overline{T_{\mathrm{g}i}}^{n+1}\left(\frac{1}{\Delta\tau}+\frac{2}{\Delta x^2\mathrm{Pe_h}}+\frac{1}{\Delta x}+\gamma_1+\gamma_2\right) = \overline{T_{\mathrm{g}i}}^{n+1}\frac{1}{\Delta x^2\mathrm{Pe_h}}+\overline{T_{\mathrm{g}i-1}}^{n+1}\left(\frac{1}{\Delta x}+\frac{1}{\Delta x^2\mathrm{Pe_h}}\right)+\frac{\overline{T_{\mathrm{g}i}}^{n}}{\Delta\tau} +\gamma_1\overline{T_{\mathrm{s}i}}^{n+1}+\gamma_2\overline{T_{\mathrm{w}i}}^{n+1} \quad 2\le i\le N \tag{A8}$$

$$\overline{T_{\mathrm{g}i}}^{n+1}\left[\frac{1}{\Delta\tau}+\frac{2}{\Delta x^2\mathrm{Pe_h}}+\frac{1}{\Delta x}+\gamma_1+\gamma_2\overline{T_{\mathrm{w}i}}^{n+1} +(\Delta x\mathrm{Pe_h}-1)\left(\frac{1}{\Delta x}+\frac{1}{\Delta x^2\mathrm{Pe_h}}\right)\right] = \overline{T_{\mathrm{g}i+1}}^{n+1}\frac{1}{\Delta x^2\mathrm{Pe_h}}+\Delta x\mathrm{Pe_h}\left(\frac{1}{\Delta x}+\frac{1}{\Delta x^2\mathrm{Pe_h}}\right)+\frac{\overline{T_{\mathrm{g}i}}^{n}}{\Delta\tau}+\gamma_1\overline{T_{\mathrm{s}i}}^{n+1} +\gamma_2\overline{T_{\mathrm{w}i}}^{n+1} \quad i=1 \tag{A9}$$

$$\overline{T_{\mathrm{g}i}}^{n+1}=\overline{T_{\mathrm{g}i+1}}^{n+1} \quad i=N \tag{A10}$$

$$\overline{T_{\mathrm{s}i}}^{n+1}=\frac{1}{1+\Delta\tau\gamma_3}\left[\Delta\tau\gamma_3\overline{T_{\mathrm{g}i}}^{n+1}+\gamma_4(Q_i^{n+1}-Q_i^n)+\overline{T_{\mathrm{s}i}}^{n}\right] \tag{A11}$$

$$\overline{T_{\mathrm{w}i}}^{n+1}=\frac{1}{1+\Delta\tau\gamma_5+\Delta\tau\gamma_6}\left[\Delta\tau\gamma_5\overline{T_{\mathrm{g}i}}^{n+1}+\Delta\tau\gamma_6\overline{T_{\mathrm{a}}}+\overline{T_{\mathrm{w}i}}^{n}\right] \tag{A12}$$

($\overline{T_{\mathrm{a}}}$ can be either 1 or not 1, depending on the inlet adsorbate temperature. If column test were carried out at ambient temperature, then $\overline{T_{\mathrm{a}}}=1$, otherwise, $\overline{T_{\mathrm{a}}}\neq 1$)

$$Y_i^1=Q_i^1=0,\ \overline{T_{\mathrm{g}i}}^{1}=\overline{T_{\mathrm{s}i}}^{1}=\overline{T_{\mathrm{w}i}}^{1}=1\,(\text{for adsorption}) \quad i=1,N+1 \tag{A13}$$

$$Y_i^1=Q_i^1=\overline{T_{\mathrm{g}i}}^{1}=\overline{T_{\mathrm{s}i}}^{1}=\overline{T_{\mathrm{w}i}}^{1}=1\,(\text{for desorption}) \quad i=1,N+1 \tag{A14}$$

The discretised equations for mass and energy balances are all tridiagonal systems, which can be easily solved by the Gaussian elimination method. Assuming that all the variables (namely, $Q_i^n, Y_i^n, \overline{T_{\mathrm{g}i}}^{n}, \overline{T_{\mathrm{s}i}}^{n}, \overline{T_{\mathrm{w}i}}^{n}$ $i=1,\ N+1$) are known, the values of $Q_i^{n+1}, Y_i^{n+1}, \overline{T_{\mathrm{g}i}}^{n+1}, \overline{T_{\mathrm{s}i}}^{n+1}, \overline{T_{\mathrm{w}i}}^{n+1}$ can be obtained from Eqs.(A4)–(A14) iteratively and then the procedure is repeated until the desired degree of convergence is achieved.

To solve the above equations, a program written in FORTRAN was developed. The convergence criterion is: $|A_i^{n+1}-A_i^n/A_i^n|\le 10^{-3}$ (A can be Y, Q, $\overline{T_{\mathrm{g}}}$, $\overline{T_{\mathrm{s}}}$ or $\overline{T_{\mathrm{w}}}$).

References

[1] D.M. Ruthven, Principles of Adsorption and Adsorption Processes, John Wiley & Sons, New York, 1984.
[2] K.S. Hwang, W.K. Lee, The adsorption and desorption breakthrough behavior of carbon monoxide and carbon dioxide on activated carbon. Effect of total pressure and pressure-dependent mass transfer coefficients, Sep. Sci. Technol. 29 (14) (1994) 1857–1891.
[3] G.H. Xiu, P. Li, Prediction of breakthrough curves for adsorption of lead (II) on activated carbon fibers in a fixed bed, Carbon 38 (7) (2000) 975–981.
[4] S. Farooq, D.M. Ruthven, Dynamics of kinetically controlled binary adsorption in a fixed bed, AIChE J. 37 (2) (1991) 299–301.
[5] S. Kaguei, Q. Yu, N. Wakao, Thermal waves in an adsorption column: Parameter estimation, Chem. Eng. Sci. 40 (7) (1985) 1069–1076.
[6] S. Kaguei, L.W. Shemilt, N. Wakao, Models and experiments on adsorption columns with constant wall temperature—radially varying and radially lumped models, Chem. Eng. Sci. 44 (3) (1989) 483–491.
[7] S. Farooq, D.M. Ruthven, Heat effects in adsorption column dynamics. 1. Comparison of one- and two- dimensional models, Ind. Eng. Chem. Res. 29 (6) (1990) 1076–1084.
[8] S. Farooq, D.M. Ruthven, Heat effects in adsorption column dynamics. 2. Experimental validation of the one-dimensional model, Ind. Eng. Chem. Res. 29 (6) (1990) 1084–1090.
[9] K.E. Noll, V. Gounaris, W.S. Hou, Adsorption Technology for Air and Water Pollution Control, Lewis Publishers, Michigan, 1992.
[10] C.C. Huang, J.R. Fair, Study of the adsorption and desorption of multiple adsorbates in a fixed bed, AIChE J. 34 (11) (1988) 1861–1877.
[11] A. Malek, S. Farooq, Kinetics of hydrocarbon adsorption on activated carbon and silica gel, AIChE J. 43 (3) (1997) 761–776.
[12] K.S. Hwang, J.H. Jun, W.K. Lee, Fixed-bed adsorption for bulk component system. Non-equilibrium, non-isothermal and non-adiabatic model, Chem. Eng. Sci. 50 (5) (1995) 813–825.
[13] L. Lapidus, G.F. Pinder, Numerical Solution of Partial Differential Equations in Science and Engineering, John Wiley, New York, 1982.
[14] C. Tien, Adsorption Calculations and Modeling, Butterworth-Heinemann, Boston, 1994.
[15] L.K.P. Hsu, H.W. Haynes, Effective diffusivity by the gas chromatography technique: analysis and application to measurements of diffusion of various hydrocarbons in zeolite NaY, AIChE J. 27 (1) (1981) 81–91.
[16] N. Wakao, S. Kaguei, Heat and Mass Transfer in Packed Beds, Gordon and Breach, New York, 1982.
[17] J.M. Schork, J.R. Fair, Parametric analysis of thermal regeneration of adsorption beds, Ind. Eng. Chem. Res. 27 (3) (1988) 457–469.
[18] T. Yang, A.C. Lua, Characteristics of activated carbons prepared from pistachio-nut shells by physical activation, J. Colloid Interface Sci. 267 (2) (2003) 408–417.
[19] P.G. Gray, D.D. Do, Adsorption and desorption of gaseous sorbates on a bidispersed particle with Freundlich isotherm. III. Contribution of surface diffusion to the sorption dynamics of sulphur dioxide on activated carbon, Gas Sep. Purif. 4 (3) (1990) 149–157.
[20] J.A.C. Silva, A.E. Rodrigues, Fixed-bed adsorption of n-pentane/isopentane mixtures in pellets of 5A zeolite, Ind. Eng. Chem. Res. 36 (9) (1997) 3769–3777.